ATLAS NOTE

ATLAS-CONF-2012-148

November 9, 2012

Search for New Phenomena in the Dijet Mass Distribution updated using 13 fb^{-1} of pp Collisions at $\sqrt{s} = 8$ TeV collected by the ATLAS Detector

The ATLAS Collaboration

Abstract

The dijet mass distribution produced in LHC proton-proton collisions at a centre-of-mass energy $\sqrt{s} = 8$ TeV has been studied with the ATLAS detector using 2012 data with an integrated luminosity of 13 fb^{-1}, reaching dijet masses up to ~ 4.69 TeV. This note updates the results of ATLAS-CONF-2012-088. No resonance-like features have been observed in the dijet mass spectrum. A new 95% C.L. lower limit on the mass of excited quarks has been set at 3.84 TeV. Extended limits on the $\sigma \times \mathcal{A}$, the product of production cross section and acceptance for hypothetical narrow particles, have also been produced using simplified Gaussian models.

ATLAS-CONF-2012-148
12 November 2012

1 Introduction

A search for new resonances and interactions in two-jet (dijet) final states, using the dijet mass distribution, was presented in Ref. [1], with 5.8 fb^{-1} of 8 TeV proton-proton collision data collected by the ATLAS detector in 2012. In that study, a 95% credibility-level (C.L.) exclusion limit on the mass of excited quarks, q^*, was set at 3.66 TeV. In the same time period, the CMS Collaboration set a q^* limit of 3.19 TeV, based on 4.0 fb^{-1} of pp collision data at 8 TeV [2]. As an additional comparison, the ATLAS Collaboration has recently submitted an analysis of the full 4.8 fb^{-1} 2011 data set at 7 TeV [3] to the Journal of High Energy Physics, setting a q^* limit of 2.83 TeV.

Here we present an update of the ATLAS 2012 analysis presented in Ref. [1], using a 2012 data sample that has been extended to an integrated luminosity of 13.0 fb^{-1}. The analysis strategy remains unchanged; in the following we summarise the essential elements of the previous analysis, and then describe the changes that have been made since.

Jets are reconstructed using the anti-k_t jet clustering algorithm [4, 5] with the distance parameter, R, of 0.6. Jets are calibrated accounting for the shift in the calorimeter response caused by the presence of multiple events in each bunch crossing, and their energy is restored to the hadronic scale [6]. Events are selected where the two highest-p_{T} jets satisfy the rapidity requirement $|y| < 2.8$ along with the dijet CM rapidity requirement $|y^*| < 0.6$ [1] and the dijet mass criterion $m_{jj} > 1000$ GeV. The event trigger consists of the logical OR of two central ($|\eta| < 3.2$), single-jet triggers, used to select events having at least one large transverse energy deposition in the calorimeter. This combined trigger avoids the inefficiencies due to splitting and merging of jets, as described in Ref. [1]. The kinematic criteria restrict jets in the analysis to have a minimum p_{T}^j of 150 GeV. The maximum jet p_{T} observed is 2.34 TeV, while the highest invariant mass event has a dijet mass of 4.69 TeV.

The current study is based on the analysis of the dijet invariant mass distribution for the selected events. The background is estimated using the observed dijet mass spectrum by fitting a smooth four-parameter function to the data:

$$f(x) = p_1(1-x)^{p_2} x^{p_3+p_4 \ln x}. \tag{1}$$

The fitting function has been used by ATLAS and other experiments [7–10]. This treatment of the background greatly reduces the effects of jet energy scale uncertainties, and the luminosity uncertainty. The search for new phenomena in the dijet mass distribution reduces to the search for significant local excesses ("bumps" or "resonances") above this parameterised background.

In 2012 the LHC has delivered increased instantaneous luminosity as well as a significant number of in-time pile-up events (multiple pp collisions in the same bunch crossing) and out-of-time pile-up events (multiple pp collisions in nearby bunch crossings). In the previous analysis the effects of this pile-up were seen to be small for high-p_{T} jets, such as those considered in this analysis; and the in-time and out-of-time pile-up conditions at the LHC were rather similar throughout 2012.

The understanding of the jet energy scale and its uncertainties improved over the course of the 2012 data taking, but no substantial changes were made in the jet calibration procedure. Jet performance and identification criteria were checked with the larger dataset used for this updated study, both globally and as a function of data taking period.

2 Changes made in the current analysis

The analysis strategy was described in detail in the documentation of the previous version with 5.8 fb^{-1} [1]. In the current study, none of the selection criteria have been changed, but there have been improvements in the search and limit-setting phases of the analysis.

- In the search phase, which looks for significant local excesses, the fitting procedure was formerly based on the χ^2 test, under the assumption that the bin populations were Gaussianly distributed.

[1] In a given event, $y^* = \pm\frac{1}{2}(y_1 - y_2)$, where the rapidities of the highest p_{T} jets are denoted by y_1 and y_2.

This has been replaced by a maximum-likelihood fit that assumes Poisson distributed statistical populations, giving more stability in the low-statistics bins at high dijet mass. The revised fitting procedure has been tested using the 5.8 fb^{-1} dataset and does not significantly change the results.

- The limit-setting phase is based as before on a Bayesian analysis of $\sigma \times \mathcal{A}$, the product of the production cross section and acceptance for a hypothetical new particle decaying into dijets. In this iteration of the analysis, the background for each mass point is determined using a fit to the data of the four-parameter function as in Eq. 1, augmented by the fully simulated dijet mass distribution signal template. The latter is scaled by a multiplicative constant to be determined in the fit. This accounts for the presence of a possible signal component that could influence the background estimate.

The dominant source of uncertainty in the limit setting phase is that associated with the jet energy scale. The first estimate of the jet energy scale uncertainty was derived in 2010 [6]. It was improved in 2011 based on studies of flavour and topology uncertainties, and was extended to the forward region employing η intercalibration studies in dijet events [11]. Pile-up produces an additional source of systematic uncertainty depending on the number of primary vertices, and on the average number of interactions per bunch crossing. The first estimate of the effect of pile-up on the jet energy scale uncertainty was developed in 2011 [12], and subsequently validated with *in situ* momentum balance techniques in studies of the 2012 data.

The jet energy scale at high p_{T} was re-adjusted since the previous iteration of the analysis, leading to an increase of $\sim 2\%$ in the energy scale above 1 TeV and to a reduction of the jet energy scale uncertainty of roughly 1%. The p_{T} and η dependent jet energy scale uncertainty for calibrated jets is as low as 4% in the central detector region.

Numerous studies of event selections and jet corrections were performed to check the stability of the established procedures and the improvements. The trigger efficiency as a function of dijet mass was compared for the first and second halves of the data sample, and found to agree within statistical uncertainties. Jet quality selections from the previous analysis were validated with the entire dataset and used here. As in the case of the previous analysis, an additional correction was applied to jets affected by dead calorimeter cells and modules. A study of events with one of the two leading jets entering the dead region was used to assess the effect on the jet energy scale exploiting transverse momentum balance in dijet events. In all cases, the studies showed that uncertainties arising from all corrections were well within the jet energy scale uncertainties considered in the analysis. The effect of the jet energy resolution uncertainty was tested both on the templates and on the background estimation and found to be negligible.

3 Updated results

3.1 Background determination and search for dijet mass resonances

Fig. 1 shows the updated mass spectrum and the resulting background fit obtained using the smooth four-parameter function. The lower panel of Fig. 1 shows the significance, in number of Gaussian standard deviations, of the difference between the data and the fit in each bin. The significance is purely statistical, and based on Poisson distributions. The contents of a given bin is used to determine the p-value, the probability of the background fluctuating higher than the observed excess or lower than the observed deficit. The p-value is transformed into a significance in terms of an equivalent number of Gaussian standard deviations (the z-value) [13]. Where there is an excess (deficit) in data in a given bin,

the significance is plotted as positive (negative). In certain cases, the significance for individual bins is not plotted. [2]

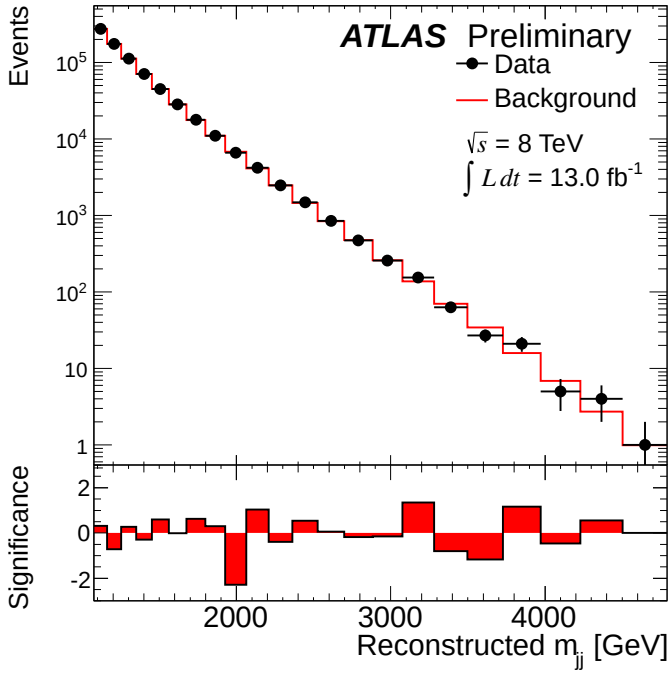

Figure 1: The reconstructed dijet mass distribution with statistical uncertainties (filled points with error bars) fitted with a smooth functional form (solid line). The bin-by-bin significance of the data-fit difference in Gaussian standard deviations is shown in the lower panel, using positive values for excesses and negative values for deficits. If a p-value greater than 50% is found the corresponding significance is not shown (see text).

The choice of dijet mass binning was motivated by the absolute resolution of the signal in the dijet mass distribution. The m_{jj} resolution was evaluated using Monte Carlo as described in Ref. [3] and it was found to improve from 7% at 1 TeV to less than 4% at 3 TeV. The analysis of the mass spectrum begins with this distribution normalised to events per bin. The maximum-likelihood fit to determine the four parameters of the smooth function is intended to be applied to a distribution in events per GeV, while retaining integer bin contents to account for Poisson statistics. The bin-width correction required to bridge these units is performed within the fitting procedure.

To test the degree of global consistency between the data and the fitted background, the p-value of the fit is determined by calculating the χ^2-value from the data and comparing this result to the χ^2 distribution obtained from pseudo-experiments drawn from the background fit, as described in the previous publication [1]. In the current analysis, the $\chi^2/\mathrm{NDF} = 15.5/18 = 0.86$, corresponding to a p-value of 0.61, showing that there is good agreement between the data and the fit.

The BumpHunter algorithm [14, 15] is used to establish the presence or absence of a localised resonance in the dijet mass spectrum, assuming Poisson statistics, and taking proper account of the "look-elsewhere effect" [16], as described in greater detail in previous publications [10, 17]. Furthermore, to prevent any new physics signal from biasing the background estimate, the region corresponding to the

[2] In mass bins with a small expected number of events, where the observed number of events is similar to the expectation, the Poisson probability of a fluctuation at least as high (low) as the observed excess (deficit) can be greater than 50%, as a result of the asymmetry of the Poisson distribution. When the significance is below zero in a bin, it is not meaningful, and the bar is not drawn in this case.

most significant local excess is excluded if the p-value of the fit is below 0.01 and a new background fit is performed. For the current dataset, no such exclusion is needed and no significant excess has been found.

3.2 Limits on excited quark production

In the absence of any observed significant discrepancy with the zero-signal hypothesis, the Bayesian method documented in the original study [1] is used to set 95% C.L. upper limits on $\sigma \times \mathcal{A}$, for a hypothetical narrow new particle decaying into dijets. As in the original study, MC samples at 8 TeV have been generated for a set of discrete q^* masses ranging from 1000 to 6000 GeV with Pythia 8 [18] using the MC12 AU2 tune [19] with the CT10 PDFs [20]. The acceptance includes reconstruction and trigger efficiencies, which are typically near 100%. For q^*, the acceptance $\mathcal{A}$ ranges from 11% to 54% for m_{q^*} varying from 1 TeV to 4.25 TeV, and is never lower than 48% for masses above 2 TeV. The main impact on the acceptance comes from the rapidity selection criteria.

The summary plot from the limit-setting analysis is shown in Fig. 2. The observed (expected) lower limit on the mass of excited quarks is 3.84 TeV (3.70 TeV). The worsening of the limit at the 5 TeV mass point can be explained by the change in shape of the simulated q^* signal, due to the rapidly decreasing parton luminosities as the dijet mass approaches the kinematic limit.

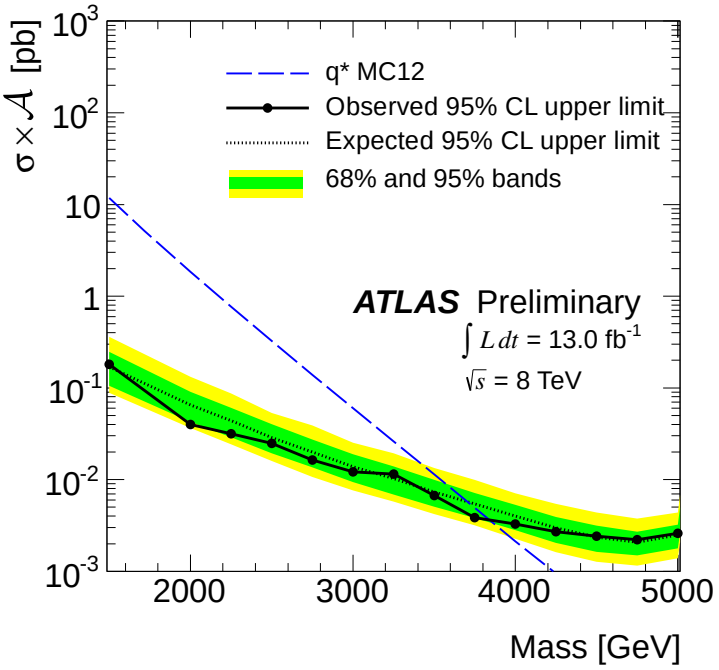

Figure 2: The 95% C.L. upper limit on $\sigma \times \mathcal{A}$ as a function of dijet resonance mass (black filled circles). The black dotted curve shows the expected 95% C.L. upper limit and the green (darker) and yellow (lighter) bands represent the 68% and 95% contours of the expected limit, respectively. The blue dashed curve represents the excited-quark $\sigma \times \mathcal{A}$ prediction.

3.3 Limits on simplified Gaussian models

As in Ref. [1] we also set limits on simplified Gaussian models, to facilitate comparisons with other new physics (NP) models beyond those considered in the current studies. Gaussian distributions of reconstructed dijet mass are added to the background estimation, for various means and widths. Upper 95% C.L. limits on $\sigma \times \mathcal{A}$ are set taking into account systematic uncertainties. The behaviour of the limits

for the different widths is driven by the increased sensitivity to single-bin fluctuations for the narrower (7%) signals.

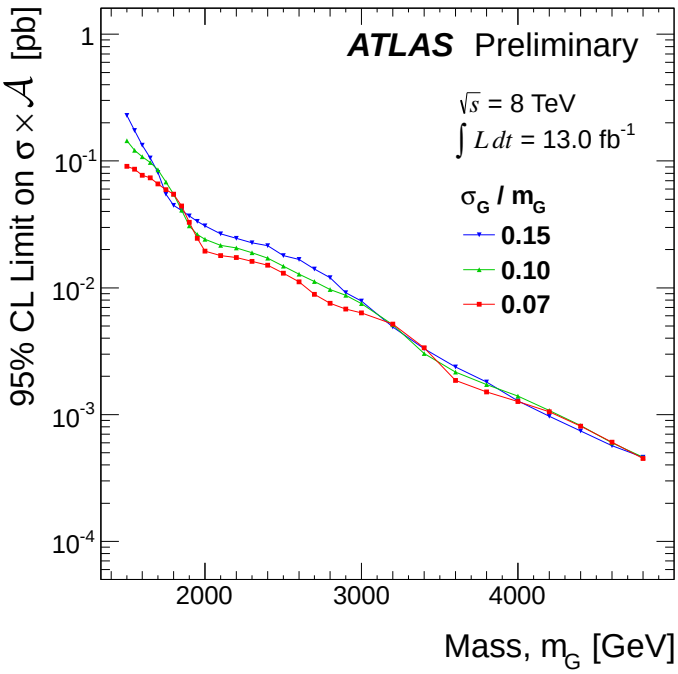

Figure 3: The 95% C.L. upper limits on $\sigma \times \mathcal{A}$ for a simple Gaussian resonance decaying to dijets as a function of the mean mass, m_{G}, for three values of $\sigma_{\mathrm{G}}/m_{\mathrm{G}}$, taking into account both statistical and systematic uncertainties.

The resulting limits on $\sigma \times \mathcal{A}$ are shown in Fig. 3 and detailed in Table 1. This analysis may be used under the condition that the NP signal shape approaches a Gaussian distribution after applying the kinematic selection criteria to y^*, m_{jj} and η of the leading jets. The acceptance should include the branching ratio of the particle decaying into dijets and the physics selection efficiency. The ATLAS m_{jj} resolution is about 5%, hence NP models with a width smaller than 7% should be compared to the 7% column of Table 1. Models with a greater width should use the column that best matches their width. A detailed description of the recommended analysis procedure, including the treatment of detector resolution effects, is given in Ref. [17]. [3]

4 Conclusions

An update of the search for new particles decaying into dijets is presented, based on an integrated luminosity of 13.0 fb^{-1} collected in 2012 with the ATLAS detector from pp collisions at 8 TeV center-of-mass at the LHC. No substantial changes were made to the previous analysis. No resonance-like features have been observed in the dijet mass spectrum. A new 95% C.L. exclusion limit on the mass of excited quarks has been set at 3.84 TeV. Limits on $\sigma \times \mathcal{A}$ for simplified Gaussian resonances have also been extended.

[3]The primary difference with respect to Ref. [17] lies in the recovery of the problematic calorimeter regions: there is no longer need for the acceptance correction described in the reference.

Table 1: The 95% C.L. upper limit on $\sigma \times \mathcal{A}$ [pb] for the Gaussian model. The symbols m_G and σ_G are, respectively, the mean mass and standard deviation of the Gaussian.

m_G	σ_G/m_G		
(GeV)	7%	10%	15%
1500	0.091	0.14	0.23
1550	0.086	0.12	0.17
1600	0.077	0.11	0.13
1650	0.074	0.097	0.11
1700	0.066	0.085	0.081
1750	0.059	0.068	0.055
1800	0.055	0.055	0.045
1850	0.044	0.041	0.041
1900	0.033	0.031	0.037
1950	0.025	0.026	0.033
2000	0.019	0.024	0.031
2100	0.018	0.022	0.027
2200	0.017	0.021	0.025
2300	0.016	0.019	0.023
2400	0.015	0.017	0.021
2500	0.013	0.015	0.018
2600	0.011	0.013	0.017
2700	0.0089	0.011	0.014
2800	0.0075	0.0097	0.012
2900	0.0068	0.0087	0.0091
3000	0.0063	0.0075	0.0079
3200	0.0052	0.0051	0.0049
3400	0.0034	0.0030	0.0033
3600	0.0019	0.0022	0.0024
3800	0.0015	0.0017	0.0018
4000	0.0013	0.0014	0.0013
4200	0.0010	0.0011	0.00097
4400	0.00081	0.00082	0.00074
4600	0.00061	0.00060	0.00057
4800	0.00045	0.00046	0.00046

References

[1] ATLAS Collaboration, *Search for New Phenomena in the Dijet Mass Distribution using 5.8 fb^{-1} of pp Collisions at $\sqrt{s}$ = 8 TeV collected by the ATLAS Detector*, ATLAS-CONF-2012-088, 2012.

[2] CMS Collaboration, *Search for Narrow Resonances using the Dijet Mass Spectrum in pp Collisions at $\sqrt{s}$ = 8 TeV*, CMS PAS EXO-12-016, 2012.

[3] ATLAS Collaboration, *ATLAS search for new phenomena in dijet mass and angular distributions using pp collisions at $\sqrt{s}$ = 7 TeV*, submitted to JHEP (2012) , arXiv:1210.1718 [hep-ex].

[4] M. Cacciari, G. P. Salam, and G. Soyez, *The anti-k_t jet clustering algorithm*, JHEP **04** (2008) 063, arXiv:0802.1189 [hep-ph].

[5] M. Cacciari and G. P. Salam, *Dispelling the N^3 myth for the k_t jet-finder*, Phys. Lett. **B641** (2006) 57, arXiv:0512210 [hep-ph].

[6] ATLAS Collaboration, *Jet energy measurement with the ATLAS detector in proton-proton collisions at $\sqrt{s}$ = 7 TeV*, accepted by EPJC (2011) , arXiv:1112.6426 [hep-ex].

[7] CDF Collaboration, *Search for new particles decaying into dijets in $p\bar{p}$ collisions at $\sqrt{s}$ = 1.96 TeV*, Phys. Rev. **D79** (2009) 112002, arXiv:0812.4036 [hep-ex].

[8] ATLAS Collaboration, *Search for New Particles in Two-Jet Final States in 7 TeV Proton-Proton Collisions with the ATLAS Detector at the LHC*, Phys. Rev. Lett. **105** (2010) 161801, arXiv:1008.2461 [hep-ex].

[9] CMS Collaboration, *Search for Dijet Resonances in 7 TeV pp Collisions at CMS*, Phys. Rev. Lett. **105** (2010) 211801, arXiv:1107.4771 [hep-ex].

[10] ATLAS Collaboration, *Search for New Physics in Dijet Mass and Angular Distributions in pp Collisions at $\sqrt{s}$ = 7 TeV Measured with the ATLAS Detector*, New Journal of Physics **13** (2011) 053044, arXiv:1103.3864 [hep-ex].

[11] ATLAS Collaboration, *In situ jet pseudorapidity intercalibration of the ATLAS detector using dijet events in $\sqrt{s}$ = 7 TeV proton-proton 2011 data*, ATLAS-CONF-2012-124, 2012.

[12] ATLAS Collaboration, *Pile-up corrections for jets from proton-proton collisions at $\sqrt{s}$=7 TeV in ATLAS in 2011*, ATLAS-CONF-2012-064, 2012.

[13] G. Choudalakis and D. Casadei, *Plotting the Differences Between Data and Expectation*, Eur. Phys. J. Plus (2012) 25, arXiv:1111.2062v3 [physics.data-an].

[14] CDF Collaboration, *Global Search for New Physics with 2.0 fb^{-1} at CDF*, Phys. Rev. **D79** (2009) 011101, arXiv:0809.3781 [hep-ex].

[15] G. Choudalakis, *On hypothesis testing, trials factor, hypertests and the BumpHunter*, arXiv:1101.0390 [physics.data-an].

[16] L. Lyons, *Open statistical issues in Particle Physics*, Ann. Appl. Stat. **2** (2008) 887.

[17] ATLAS Collaboration, *Search for new physics in the dijet mass distribution using 1 fb^{-1} of pp collision data at $\sqrt{s}$ = 7 TeV collected by the ATLAS detector*, Phys. Lett. **B708** (2012) 37, arXiv:1108.6311 [hep-ex].

[18] T. Sjostrand, S. Mrenna, and P. Z. Skands, *A Brief Introduction to PYTHIA 8.1*, Comput. Phys. Commun. **178** (2008) 852–867, arXiv:0710.3820 [hep-ph].

[19] ATLAS Collaboration, *Further ATLAS tunes of Pythia 6 and Pythia 8*, ATL-PHYS-PUB-2011-014, 2011.

[20] P. M. Nadolsky et al., *New parton distributions for collider physics*, Phys. Rev. **D82** (2010) 074024, arXiv:1007.2241 [hep-ph].

Appendices

A Comparison of signal and data with background prediction

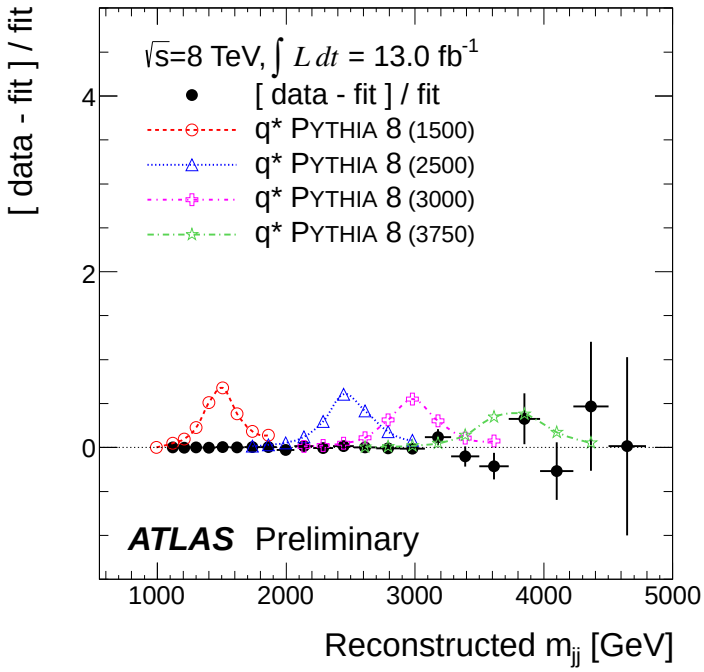

Figure 4: Four predicted excited quark (q^*) mass templates, normalised to the integrated luminosity, are compared to the data. The q^* templates and data are plotted as ratios relative to the background fit.

B Event displays of the highest dijet mass event

Figures 5 and 6 show the event display for the highest-mass and highest-transverse-momentum dijet events entering the HCP analysis (m_{jj}=4.69 TeV, event number 179229707, run 209580 and p_T = 2.34 TeV, event number 37979867, run 208781).

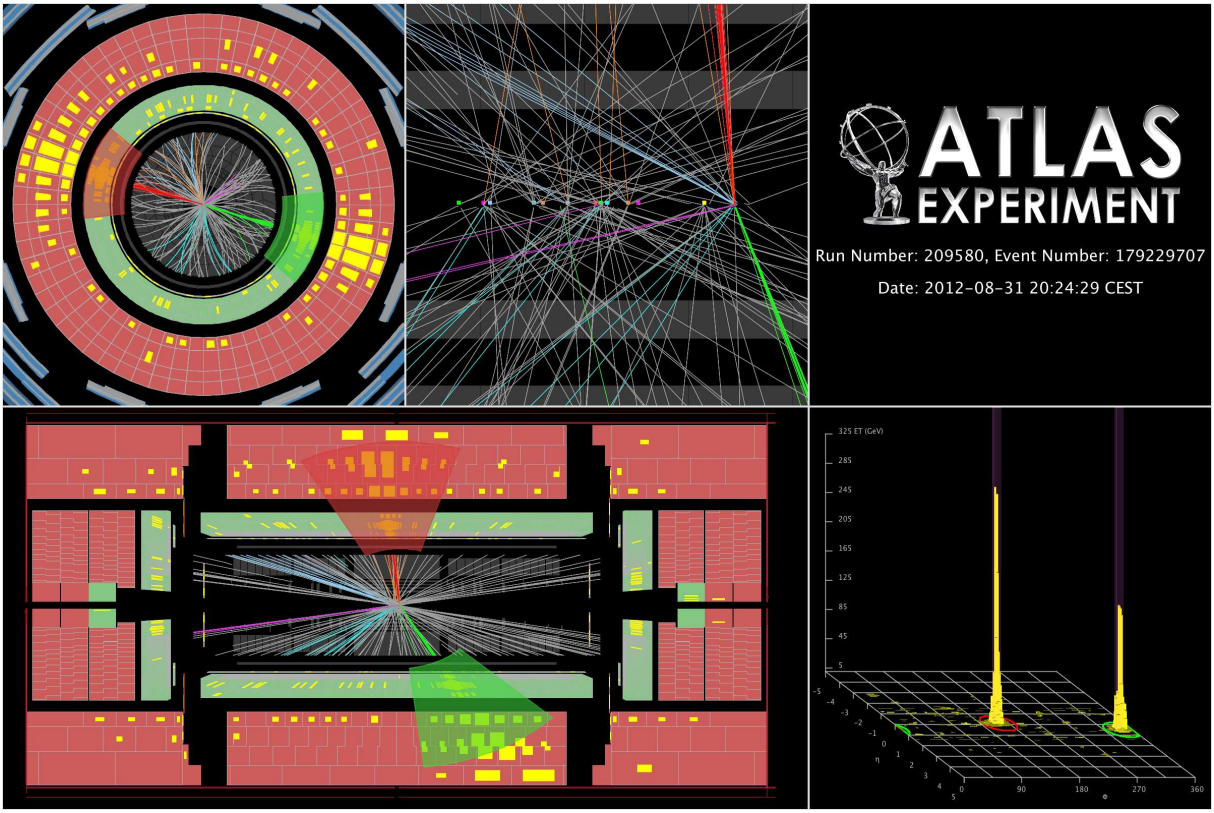

Figure 5: The highest-mass central dijet event collected by the end of September 2012 (Event 179229707, Run 209580): the two central high-p_T jets have an invariant mass of 4.69 TeV, and the highest-p_T jet has a p_T of 2.29 TeV, and the subleading jet has a p_T of 2.19 TeV. The missing E_T and Sum E_T for this event are respectively 47 GeV and 4.85 TeV. Only tracks with $p_T > 0.7$ GeV are displayed. The event was collected on August 31st, 2012.

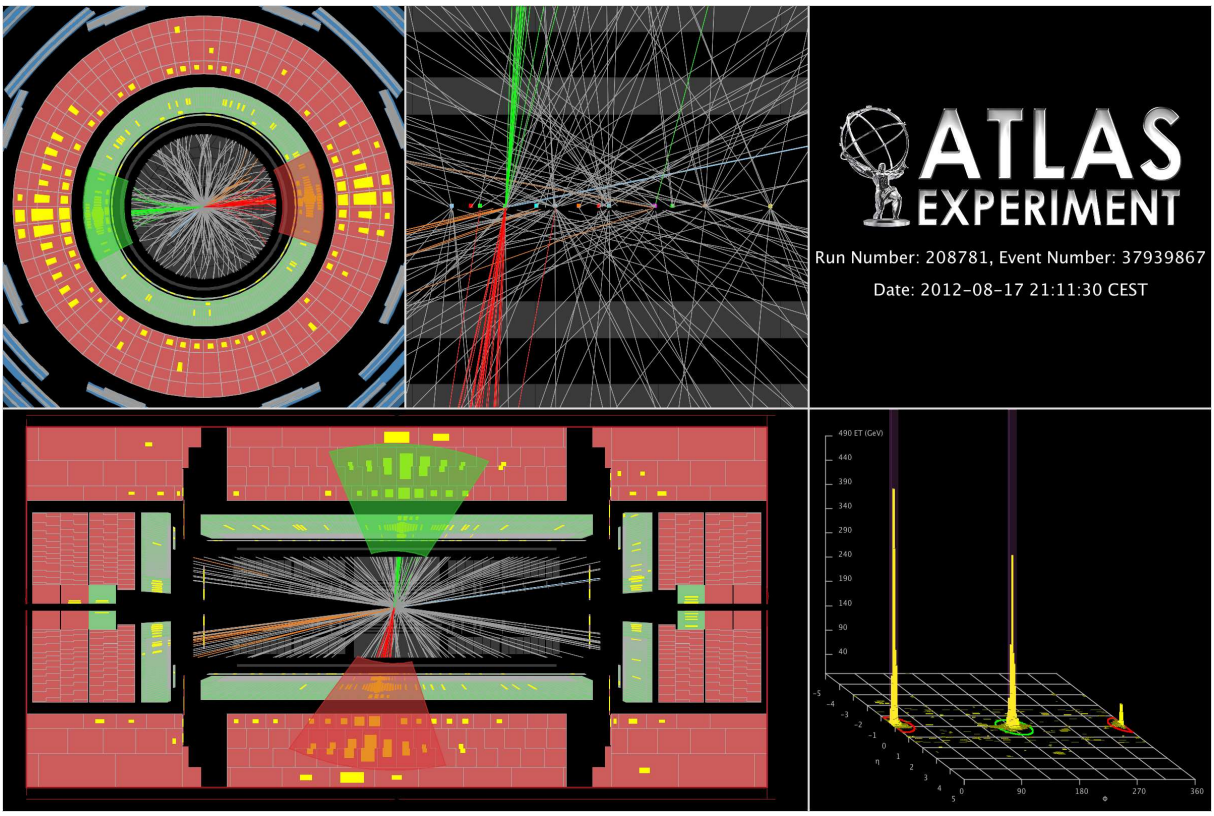

Figure 6: The highest-p_{T} jet event collected by the end of September 2012 (Event 37979867, Run 208781): the two central high-p_{T} jets have an invariant mass of 4.47 TeV, and the highest-p_{T} jet has a p_{T} of 2.34 TeV, and the subleading jet has a p_{T} of 2.10 TeV. The missing E_T and Sum E_T for this event are respectively 115 GeV and 4.97 TeV. Only tracks with $p_T > 0.7$ GeV are displayed. The event was collected on August 17$^{\mathrm{th}}$, 2012.